Quantifying Uncertainties in Determining SW Cloud Radiative Forcing and Cloud Absorption due to Variability in Atmospheric Conditions

ZHANQING LI* AND ALEXANDER P. TRISHCHENKO

Canada Centre for Remote Sensing, Ottawa, Ontario, Canada

(Manuscript received 10 January 2000, in final form 2 June 2000)

ABSTRACT

The concept of cloud radiative forcing (CRF) has been widely employed in studying the effects of clouds on the earth's radiation budget and climate. CRF denotes, in principle, the net influence of cloud alone on the radiation budget of a system. In practice, however, observational determination of CRF is fraught with uncertainties due to factors other than cloud that induce changes in atmospheric background conditions. The most notable variables include aerosol, water vapor, and the data sampling scheme. The impact of these factors on the derivation of CRF and cloud absorption is investigated here by means of modeling and analysis of multiple datasets. Improved estimation of CRF is attempted at the top of the atmosphere (TOA) and at the surface from spatially and temporally collocated ground and satellite measurements for broadband shortwave fluxes. Satellite data employed include pixel measurements from ERBE (1988–90), ScaRaB (1994–95), and CERES (1998), as well as surface data acquired across the Canadian radiation network, the ARM Central Facility site in Oklahoma, the US/NOAA SURFRAD networks, and the world BSRN (WMO) networks. It is found that surface CRF is much more susceptible to the variability in background conditions than TOA CRF. Selection of overly clear sky conditions often leads to significant overestimation of surface CRF, but TOA CRF remains intact or only slightly affected. As a result, the ratio of CRF at the surface and TOA is prone to overestimation. With careful treatments of these effects, the CRF ratio turns out to vary mostly between 0.9 and 1.1, implying approximately the same magnitude of atmospheric absorption under clear-sky and cloudy-sky conditions.

1. Introduction

Clouds play critical roles in dictating the earth's energy and water cycles and thus influence the earth's climate most significantly (Arking 1991; Liou 1992; Stephens 1999). The earth–atmosphere energy balance is governed primarily by interactions between clouds and the radiation budget, while other factors such as water vapor and aerosol also play important roles (Hartman et al. 1986). The mechanisms by which the interactions takes place are extremely complex and involve seven independent cloud variables acting on a hierarchy of spatial and temporal scales (Wielicki et al. 1996). One aspect of the interaction can, however, be described by a single quantity, namely, the cloud radiative forcing (CRF) (Charlock and Ramanathan 1985). A major advantage of using CRF is that its value can be obtained directly from satellite observation at the top of the atmosphere (TOA) (Ramanathan et al. 1989; Harrison et al. 1990), as well as at the surface by means of satellite inversion (Li and Leighton 1993; Zhang et al. 1995; Rossow and Zhang 1995).

The observed CRF is proven to be instrumental in diagnosing climate models (Cess et al. 1997; Barker et al. 1994; Li et al. 1997). Comparing the magnitudes and trends of the variation in CRF as derived from satellite and modeled by general circulation models, one may identify drawbacks in the treatment of clouds and cloud–radiation interaction. However, such comparisons suffer from some inherent uncertainties. A major uncertainty arises from the compatibility between satellite-derived and model-computed CRF. In theory, the CRF determined either from a model or observation is supposed to denote the radiative effects of clouds alone, but in practice it is influenced by factors other than clouds. A major influence is the variability in clear-sky background conditions. Major factors affecting clear-sky fluxes include aerosol and water vapor. Since it is not possible to measure the background clear-sky fluxes under cloudy conditions, determination of the clear-sky reference value is one of the major sources of uncertainty in determining CRF from observational data.

The uncertainties in determining CRF at the surface and at the TOA may jeopardize the accuracy of the CRF ratio that has been employed in many recent studies on

* Current affiliation: Department of Meteorology, Earth System Science Interdisciplinary Center, University of Maryland, College Park, Maryland.

Corresponding author address: Dr. Z. Li, Canada Centre for Remote Sensing, 588 Booth Street, Ottawa, ON K1A 0Y7, Canada.
E-mail: li@ccrs.nrcan.gc.ca

the so-called cloud absorption anomaly (CAA) issue (Stephens and Tsay 1990). The essence of the debate is whether clouds *substantially* alter the solar radiation budget in the atmospheric column. Ramanathan et al. (1995) estimated CRF over the tropical warm pool region and found that CRF at the TOA is a factor of 1.5 larger than that at the surface, while conventional radiative transfer theories predict similar magnitude of CRF at the two levels (Li et al. 1997). This finding implies that clouds absorb much more solar radiation than models predict. Cess et al. (1995) reinforced the finding by analyzing satellite and surface measurements made over several other locations. In both studies, CRF was estimated and compared at the TOA and at the surface. Following a similar approach, Li et al. (1995) drew a different conclusion by analyzing 4 yr of gridded monthly mean satellite data from the Earth Radiation Budget Experiment (ERBE) and from the Global Energy Balance Archive. They found that the CRF ratio is generally around unity except for some tropical areas in certain months. The exceptions were later found to be caused by inadequate estimation of clear-sky reference values due to the existence of smoke aerosol (Li 1998). After correcting for the smoke effect, the CRF ratio becomes close to unity. In light of the sensitivity of CRF to the identification of clear skies, Chou and Zhao (1997) designed a meticulous procedure for identifying clear skies. With a more reliable scene identification, Chou et al. (1998) recomputed the CRF and its ratio in the warm region and found that the ratio was around 1.1. Arking (1999a,b) argued that the effect of water vapor on atmospheric absorption may not be accounted for properly in determining the background offset value that may be mistakenly attributed to a cloud effect. The debate is still ongoing following a recent experiment named ARESE that was dedicated to addressing this issue. Using data from the experiment, findings in favor (Valero et al. 1997; Zender et al. 1997; Cess et al. 1999) and against (Li et al. 1999) the CAA theory were reported. While data quality is at the heart of the debate, analysis methodology could be a contributing factor that is worth thorough and painstaking scrutiny.

The current investigation is therefore devoted to a thorough evaluation of major uncertainties in determining CRF at the surface and TOA and their ratio by means of model simulation and analyses of extensive datasets. The datasets employed in the study are described in section 2. A general discussion on terminology and sources of uncertainty in each variable of concern is given in section 3. Section 4 presents some modeling results to quantify the magnitudes of bias errors due to various parameters. Analyses of observational data are presented in section 5. Section 6 summarizes our conclusions.

2. Datasets

Several satellite and surface datasets are employed in this study. The surface data were collected at the Atmospheric Radiation Measurement (ARM) Central Facility (CF) site, the Canadian radiometer network, the Baseline Surface Radiation Network (BSRN), and the U.S. National Oceanic and Atmospheric Administration's (NOAA's) Surface Radiation (SURFRAD) network. Satellite data are from three space programs measuring the earth's radiation budget, namely, the ERBE, the Scanner for Radiation Budget (ScaRaB), and the Cloud and Earth Radiant Energy System (CERES).

ARM provides long-term extensive observations concerning the radiative environment of the atmosphere, cloud, and surface. Many state-of-the-art instruments were deployed on the ground, supplemented with aircraft and spacecraft measurements. Data obtained at the ARM Southern Great Plains (SGP) site in Oklahoma are employed here as they are most complete and cover a long period of time overlapped with satellite observations. The datasets include surface radiative fluxes (total, direct, and diffuse) measured by the BSRN system, atmospheric precipitable water (PW) retrieved from the microwave radiometer (MWR), and aerosol optical depth obtained from the Multi-Filter Rotating Shadowband Radiometer (Harrison et al. 1994; Michalsky et al. 1999). The temporal sampling interval of the original datasets is 1 min, except for data from the SURFRAD, whose sampling interval is 3 min. The data were averaged to 30-min means that were matched to satellite observations. Although satellite data are instantaneous, they represent aerial means over much larger areas than the surface data. Temporal averaging of the ground measurements would partially compensate for the discrepancies in time and space with satellite data.

The Canadian radiation data were acquired and maintained by the Canadian Atmospheric Environment Service (AES). While there are tens of radiation stations operating in Canada, data from most stations were archived as hourly means. Data of 1-min intervals at five stations are analyzed in this study. The observations were made with CM6 Kipp pyranometers. The calibration uncertainty was believed to be within 5%. The locations of the stations are given in Table 1, and their spatial distribution can be seen in Barker et al. (1998). Data from three SURFRAD stations in the United States (cf. Table 1) were also employed. SURFRAD is a ground-based radiation network operated by NOAA (Augustine et al. 2000). The locations were chosen over relatively uniform areas. There are several radiometers deployed at each SURFRAD station measuring total, direct, diffuse, UV, and spectral irradiances, etc. The calibration was well maintained to within 15 W m^{-2} for 99% of the measurements. BSRN is a worldwide network for acquiring high quality surface radiation data (Ohmura et al. 1998). Currently, there are 30 BSRN stations in operation, but very few have provided their data, which were made available for use here, to the BSRN archival.

It is worth noting that an increasing attention has been

TABLE 1. The list of surface radiation stations used in this study.

No.	Station name	Operating agencies	Lat (North)	Long (East)	Observation period	Satellite project
1	Port Hardy	AES, Canada	50.68°	232.63°	1988–90, 1994–95	ERBE, ScaRaB
2	Stony Plains	AES, Canada	53.53°	245.99°	1988–90, 1994–95	ERBE, ScaRaB
3	Winnipeg	AES, Canada	49.90°	262.77°	1988–90, 1994–95	ERBE, ScaRaB
4	Dorval	AES, Canada	45.47°	286.25°	1988–90, 1994–95	ERBE, ScaRaB
5	Goose Bay	AES, Canada	53.30°	299.63°	1988–90, 1994–95	ERBE, ScaRaB
6	ARM SGP CF, Oklahoma	DOE ARM	36.60°	262.52°	1994–95, 1998	ScaRaB, CERES
7	Boulder	SURFRAD, NOAA	40.216°	254.6°	1994–95, 1998	ScaRaB, CERES
8	Bondville	SURFRAD, NOAA	40.1°	271.383°	1994–95, 1998	ScaRaB, CERES
9	Goodwin Creek	SURFRAD, NOAA	34.25°	270.133°	1994–95, 1998	ScaRaB, CERES
10	Payerne	BSRN, WMO	46.82°	6.93°	1994–95	ScaRaB

called for concerning uncertainties in the calibration of some types of pyranometers due to the thermal effect of the pyranometer's dome. Both observational (Bush et al. 2000) and modeling studies (Ji and Tsay 2000) showed that the dome effect could cause a measurement uncertainty of over 5∼10 W m^{-2}. Moreover, the effect is larger under clear-sky conditions than under cloudy ones (Dutton et al. 1999), which could have an adverse impact on the current analysis. Unfortunately, it is unfeasible to quantify this uncertainty and correct it for historical data as it requires observations of temperatures for the dome and the sensor, although some laboratory tests have been carried out (Haeffelin et al. 1999).

ERBE, ScaRaB and CERES provided onboard calibrated shortwave (SW) and longwave (LW) radiative flux measurements over different periods of time at different spatial resolutions: ∼20 km (CERES), 40 km (ERBE), and 60 km (ScaRaB). ERBE provided the longest record of data from 1985 to 1990 from its scanning radiometers (Barkstrom et al. 1989). ScaRaB observation lasted about 1 yr from February 1994 through March 1995 (Kandel et al. 1998; Trishchenko and Li 1998a). The CERES on board the Tropical Rainfall Measuring Mission satellite provided a limited amount of data from the end of December 1998 to the end of August 1998. Its operation may resume after the Earth Observing System *Terra* is launched. These satellite measurements are used to derive TOA CRF. In our study we employed ERBE-like version of CERES data available from the National Aeronautics and Space Administration Langley Research Center archive for the first 8 months of 1998.

Except for the ARM site, water vapor data at all other stations were taken from the National Centers for Environmental Prediction (NCEP)–National Center for Atmospheric Research (NCAR) reanalysis (Kalnay et al. 1996). They were derived by combining observations from radiosonde and satellite retrievals, as well as from model assimilation. Over most land sites, radiosonde may be the sole source of water vapor observations, especially in older analyses. Despite some shortcomings related to the deficiencies associated with model assumptions, satellite retrievals and lack of measurements over broad land areas, the reanalysis is among the best and consistent global uniform datasets available at present. The data are available with temporal resolution of 6 h and spatial lat–lon grid of 2.5° × 2.5°.

When a CRF derived from satellite was compared to CRF at the surface, only data with simultaneous satellite and ground observations were employed. The maximum allowed distance between the center of a satellite pixel and the location of a surface station was 20 km for ERBE and ScaRaB data (approximately half of their pixel size) and 10 km for CERES. Ground measurements were averaged over 30-min intervals centered at the satellite observations.

Determination of surface cloud radiative forcing also requires surface albedo whose measurements at the ground are scanty and not representative over the large areas of satellite pixels. We therefore estimate its values from clear-sky satellite observations using the algorithm of Li and Garand (1994). Calculation of surface net flux for all-sky conditions would require a knowledge of surface albedo under cloudy conditions as well. To understand and correct for the dependence of albedo on cloudiness, model calculations were conducted for different cloud optical thickness and heights over various surface types. Both modeling results and observations made at the ARM SGP site show that surface albedos under overcast conditions depend very weakly on cloud optical depth and height. Its magnitude is approximately equal to the average of clear-sky values with the cosine of the solar zenith angle (SZA) greater than 0.6 at an accuracy of about 2%–3%. Surface albedos for partially cloudy scenes (cloud amount 5%–50%) and mostly cloudy (50%–95%) scenes as classified by ERBE, ScaRaB, and CERES were computed from the following approximations:

$$\alpha = \frac{3}{4}\alpha_{\text{clear-sky}} + \frac{1}{4}\alpha_{\text{cloudy}} \quad \text{for partly cloudy scenes,}$$

$$\alpha = \frac{1}{4}\alpha_{\text{clear-sky}} + \frac{3}{4}\alpha_{\text{cloudy}} \quad \text{for mostly cloudy scenes.}$$

TABLE 2. Statistics of precipitable water vapor under different sky conditions.

Station name	Clear			Partly cloudy			Mostly cloudy			Overcast		
	m	σ	N	m	σ	N	m	σ	N	m	σ	N
Port Hardy, ERBE	1.23	0.48	569	1.30	0.46	952	1.48	0.52	1339	1.74	0.60	762
Stony Plain, ERBE	0.97	0.44	650	1.05	0.51	1585	1.13	0.55	1079	1.26	0.51	699
Winnipeg, ERBE	1.66	0.69	742	1.73	0.82	1186	1.82	1.08	866	2.13	1.11	428
Dorval, ERBE	1.61	0.85	235	1.77	0.99	978	1.88	1.06	917	2.21	1.05	418
Goose Bay, ERBE	1.33	0.57	458	1.40	0.74	780	1.66	0.73	1180	1.97	0.74	595
SGP ARM, CERES	2.62	1.23	787	2.50	1.36	825	2.43	1.46	418	3.02	1.47	311
SGP ARM, CERES, Jan, MWR data	1.20	0.41	26	1.98	0.33	58	1.83	0.25	117	1.86	0.68	33
SGP ARM, CERES, Mar, MWR data	1.18	0.28	135	1.23	0.39	168	1.48	0.60	104	2.36	0.67	56
SGP ARM, CERES, Jul, MWR data	3.98	0.49	140	4.37	0.49	274	4.84	0.60	132	4.85	0.60	62

3. Cloud radiative forcing and its ratio: Definition and uncertainty

Let us denote the net flux at the TOA (surface) level as

$$T(S) = F^{T(S)}\downarrow - F^{T(S)}\uparrow = (1 - \alpha^{T(S)})F^{T(S)}\downarrow,$$

and define cloud radiative forcing as

$$C^{T(S)} = T(S) - T(S)^{\mathrm{CLR}},$$

where $\alpha^{T(S)}$ is TOA (surface) albedo, $F\uparrow$ ($F\downarrow$) is upward (downward) flux. The index ''CLR'' denotes clear-sky scenes, that is, the atmosphere without cloud or cloud having been removed. To estimate the CRF over a period of time, average quantities are employed:

$$C^{T(S)} = \frac{1}{N}\sum_i (T(S)_i - T(S)_i^{\mathrm{CLR}}). \quad (1)$$

Note that the quantities, T and T^{CLR} or S and S^{CLR}, cannot be observed simultaneously for each observational moment ''i.'' Each observation corresponds to either a clear or a cloudy condition. As a result, an observed CRF is actually given by

$$O^{T(S)} = \frac{1}{N}\sum_i T(S)_i - \frac{1}{N_{\mathrm{CLR}}}\sum_{i\in \mathrm{CLR}} T(S)_i^{\mathrm{CLR}}, \quad (2)$$

where the second term is for clear-sky observations only.

The difference between an ''intended'' and ''observed'' CRF is

$$\Delta^{T,S} = C^{T,S} - O^{T,S} = (1 - P_{\mathrm{CLR}})(\Psi^{T,S} - \Omega^{T,S}), \quad (3)$$

where p_{CLR} is the probability of clear-sky scenes, $\Psi^{T,S} = (1/N_{\mathrm{CLR}})\ \Sigma_{i\in \mathrm{CLR}}\ T(S)^{\mathrm{CLR}}$ is an observed mean clear-sky net flux, and $\Omega^{T,S} = (1/N_{\mathrm{CLR}})\ \Sigma_{i\in \mathrm{CLR}}\ T(S)_i^{\mathrm{CLR}}$ is a hypothetical clear-sky flux for cloudy scenes. If the two ''clear-sky'' reference values were the same, observed CRF would be identical to the CRF required. In reality, this may not be the case, as atmospheric conditions vary with cloud cover. Table 2 presents mean PW amounts under clear, overcast, and all-sky conditions obtained from the ARM archival and NCEP–NCAR reanalysis. As expected, water vapor content was the lowest under clear-sky conditions and highest for overcast skies. The difference between ''required'' and observed CRF originates from discrepancies in the atmospheric background state. If this ''radiative background'' for cloudy scenes is different from that for clear-sky scenes, a bias error is introduced. One could obtain a nonzero ''CRF'' for clear-sky scenes, if the clear-sky background chosen as reference is biased relative to the overall mean clear-sky conditions. This is especially the case for using the ''upper envelope method'' to select clear scenes corresponding to cases with the highest atmospheric transmission as noticed by Imre et al. (1996). In this case, the resulting radiative forcing actually denotes both atmospheric effects, cloud absorption, and cloud 3D effects. The former is caused by changes in atmospheric conditions for clear skies.

ARM datasets allow us to observationally estimate the magnitude of uncertainty in CRF due to variability in clear-sky background conditions. The major factors driving radiative forcing under clear-sky conditions are water vapor and aerosol (Trishchenko and Li 1998b). Their influences may be inferred from surface radiation measurements. To this end, all clear-sky surface downward solar fluxes were grouped into bins according to total water vapor amount (PW = 0–1, 1–2, 2–3 cm, etc.) and aerosol optical depth (τ = 0–0.1, 0.1–0.2, etc.). Mean fluxes were computed for each combination of PW, τ and μ_0 bins, where μ_0 is the cosine of the solar zenith angle (SZA). The overall mean flux was then subtracted from the bin fluxes averaged over μ_0. The bars in Fig. 1 show the differences for three ranges of aerosol optical depths and four intervals of PW, normalized to the mean sun–earth distance (1 AU). Since values of various SZAs were averaged, the results approximately represent daytime means. Note that the bars are not symmetric with respect to the ''0'' difference line, as the number of samples differs among the bins. The majority of measurements fell within τ = 0–0.1 and thus the bars in this interval are more symmetric than other τ intervals. The effect of the amount of water vapor is grossly denoted by the contrast between the bars in the same interval of τ, while that of aerosol can be seen by comparing bars in different clusters of τ. From the comparison of the three clusters of bars, it is evident that the aerosol effect diminishes as aerosol loading increases. It appears that the effect of water

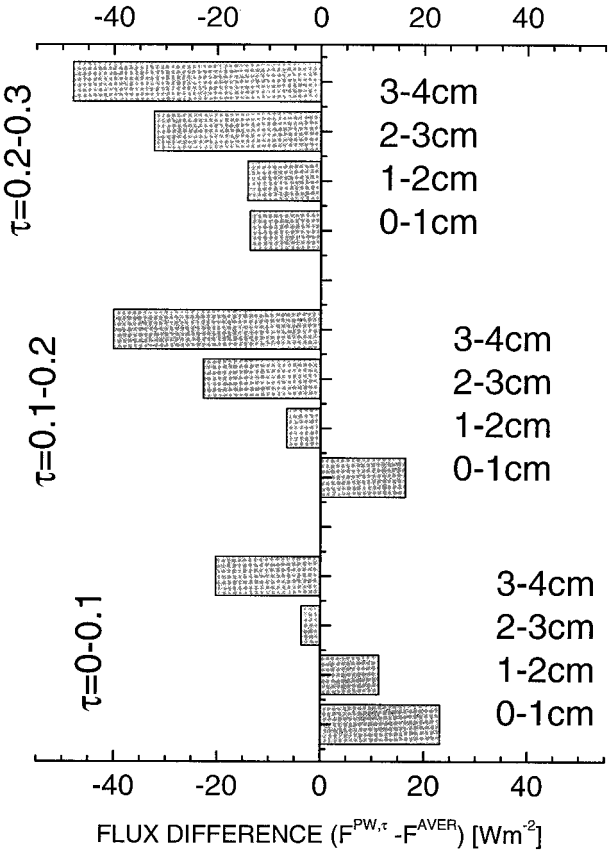

FIG. 1. Observed radiative forcing of water vapor and aerosol on surface downward solar radiation at the ARM SGP CF site in Oklahoma over the period of 1994–98. The differences were calculated with respect to the overall mean surface fluxes under all clear conditions. A total of 5012 measurements were employed that were sorted into bins of 1-cm intervals for water vapor and 0.l intervals for aerosol optical thickness observed at 500 nm. Shortwave fluxes were normalized to the mean sun–earth distance (1 AU).

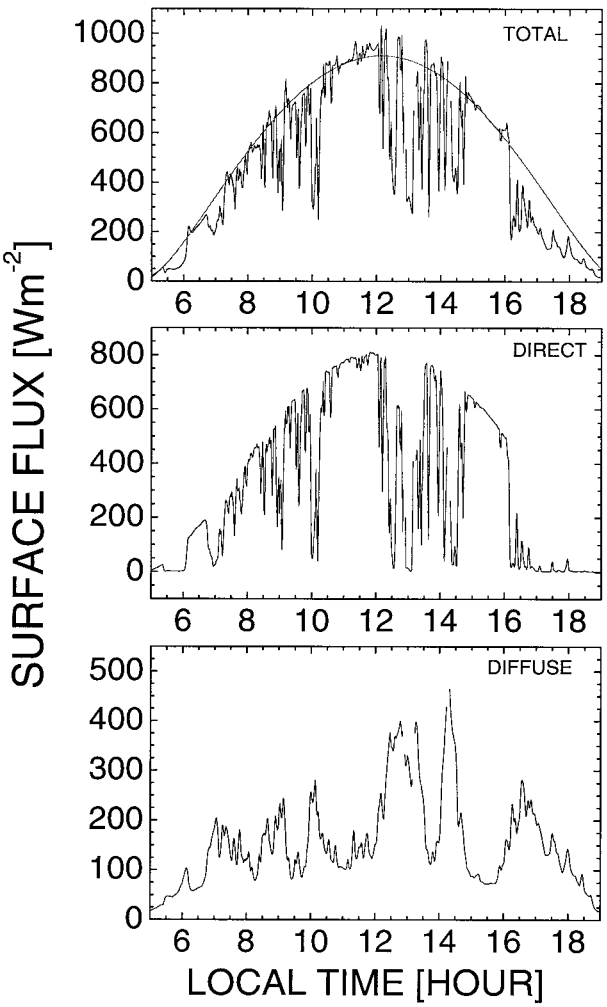

FIG. 2. Diurnal variation of surface total, direct, and diffuse fluxes for a mixed-sky condition with periods of clear, overcast, and residual clouds. The curve is a fit of clear-sky observations. The values exceeding the curve denote overshooting of photons from cloud sides. The data were measured in Winnipeg, MB, Canada, on 11 May 1988.

vapor is larger than that of aerosol. The difference between the bars for PW = 0–1 cm and PW = 3–4 cm of the same τ indicates roughly the upper limit of the radiative effect of water vapor, which is in the order of 50 W m^{-2} and has a very weak dependence on aerosol amount. Likewise, one can infer the effect of aerosol by comparing bins of τ = 0–0.1 with those of τ = 0.2–0.3 for the same amount of PW. The aerosol effect is found to vary from 25 W m^{-2} for PW = 3–4 cm to about 40 W m^{-2} for PW = 0–1 cm. These values are very significant compared to the observed daytime mean downward SW flux of ~500 W m^{-2} and to the mean CRF of around 100 W m^{-2}, which warrants a careful determination of the clear-sky reference value in deriving CRF.

Another potential problem in deriving CRF is associated with data sampling, which is related to the identification of clear-sky intervals for determining clear-sky net fluxes. Since cloud cover is a ubiquitous phenomenon, there are not many opportunities to find completely cloud-free intervals. Even for the intervals when a cloud does not block direct solar radiation, the cloud still has an influence through scattered diffuse solar radiation. Therefore under partly cloudy conditions, the downward flux or atmospheric transmittance may be higher than under clear-sky conditions for the similar vertical structure of the atmosphere. Selecting these occasions as clear-sky background artificially increases the cloud radiative forcing. The excess of surface insolation may be as large as 100–200 W m^{-2} and is a common event, as shown in Fig. 2. There are many moments when clouds do not block the sun and thus the direct radiation remains the same as if the entire sky dome were cloud free, but the diffuse component is enhanced considerably. The duration of truly cloud-free sky is rather short. Following the method of identifying clear skies using ground-based observations of total, direct,

and diffuse fluxes similar to Chou and Zhao (1997; also described in section 4), we found that typically only one-third of ERBE designated ''clear over land'' scenes passed through the clear-sky tests. This finding is also consistent with that of using an alternative scheme of clear-sky identification adopted from the approach proposed by Long and Ackerman (1996). The remaining two-thirds of ''clear'' scenes as identified by ERBE actually contain some fractions of clouds. Therefore the TOA CRF derived from satellite may be somewhat underestimated, due to enhanced solar reflection by residual clouds. On the other hand, if a cloud does not obscure the sun, its impacts on TOA and surface net flux are just the opposite, leading to an overestimation for surface CRF and underestimation for TOA CRF.

Errors in CRF lead to bias errors in the ratio of CRF at surface over that at the TOA. Assuming that Δ^S and Δ^T are very small relative to the true values of CRF, the ratio of CRF at the surface and that at the TOA can be expressed as

$$R = \frac{C^S}{C^T} = \frac{O^S + \Delta^S}{O^T + \Delta^T} \approx \tilde{R} + \frac{\Delta^S}{O^T} - \tilde{R}\frac{\Delta^T}{O^T}, \quad (4)$$

where $\overline{R}$ is observed CRF ratio $\overline{R} = O^S/O^T$. The difference between desired and observed R is

$$\Delta R = R - \tilde{R} = \frac{\Delta^S - \tilde{R}\Delta^T}{O^T}. \quad (5)$$

Assuming that the conventional radiative transfer theories are correct, $\overline{R}$ would be generally in the neighborhood of unity (Li et al. 1995). Assuming $\overline{R} = 1$, we have

$$\Delta R = R - \tilde{R} \approx \frac{\Delta^S - \Delta^T}{O^T}. \quad (6)$$

Therefore, the discrepancy between observed and required CRF ratio ΔR is very sensitive to the difference between CRF errors at the surface and at the TOA. In the case of residual clouds as discussed above, the CRF ratio could be substantially overestimated as they may induce errors of opposite signs in surface and TOA CRF. Overestimation of R may also occur for strong absorbing media such as water or absorbing aerosol. The influence of such media is usually larger at the surface than at the TOA. For example, for an absorbing aerosol, an increase in TOA reflection is partially compensated by its absorption in the atmosphere leading to a relatively small deviation, whereas both absorption and scattering effects reduce solar energy reaching the surface. On the other hand, for a conservative scattering aerosol, ignoring its existence may induce a significant error in determining CRF due to the aerosol forcing but has no or little impact on the ratio of CRF. This is because its radiative impact at the TOA and at the surface are of the same sign and of similar magnitudes; thus $\Delta R \approx 0$. Therefore, caution needs to be exercised in interpreting an observed CRF ratio in terms of cloud absorption, as it is dictated by many factors. This is further demonstrated in the following sections by means of modeling and analyses of observational data.

4. Model simulation of TOA and surface CRF and its ratio

To further elucidate and quantify the aforementioned effects, model simulations were conducted using an adding–doubling radiative transfer method combined with the LOWTRAN-7 atmospheric transmittance model (Masuda et al. 1995). The model has 120 unequally spaced spectral intervals between 0.25 and 22.5 μm, including 41 intervals within 0.3–1 μm, 30 within 1–2 μm, and 34 within 2–5 μm. Hemispheric fluxes in upward and downward directions are computed at 11 streams. The continental model aerosol defined in WCP-112 (WCP 1986) was adopted with different optical thickness τ ranging from 0 to 0.5 at 0.55 μm. About two-thirds of aerosol burden was concentrated in the layer below 2 km. The St I model cloud of optical thickness 40 defined by Stephens (1979) was placed in the layer between 2 and 4 km over a grassland surface. Vertical profiles of temperature, pressure, humidity, and gases corresponded to midlatitude summer (MLS) atmosphere (Kneizys et al. 1988). The impact of PW was studied by scaling the MLS water vapor profile to achieve the total amount of PW as prescribed.

a. Aerosol effect

For conservative scattering aerosols, their radiative impact bears a close resemblance to that of clouds. It has no or little effect on CRF and on the ratio of CRF at the surface and at the TOA. However, for absorbing aerosols, their impact on CRF is much more complex. They usually exert different influence under clear and cloudy conditions, as well as on surface and TOA fluxes, as is shown in Fig. 3 for the continental aerosol as an example. The aerosol has a SW cooling effect that is about 3–4 times greater at the surface level than at the TOA for clear skies. Depending on SZA, the rate of aerosol forcing is 1–6 W m^{-2} per $\Delta\tau = 0.1$ at the TOA and 10–15 W m^{-2} per $\Delta\tau = 0.1$ at the surface. For cloudy skies, however, aerosol has a SW warming effect at the TOA due to enhanced absorption and remains a cooling effect at the surface, but of considerably smaller magnitude than in clear-sky cases. The effects of aerosol on CRF and the ratio of CRF at the TOA and surface are even more complex and may be summarized in two scenarios. In the first scenario, clear and cloudy skies contain the same amount of aerosol. Although such a scenario is ideal for determining the sole effect of cloud on radiation as designated by CRF, it is worth emphasizing that the resulting CRF is still contingent upon the amount of aerosol. It follows from Fig. 4 that increasing aerosol loading decreases CRF at both the TOA and surface levels because of a reduced contrast between

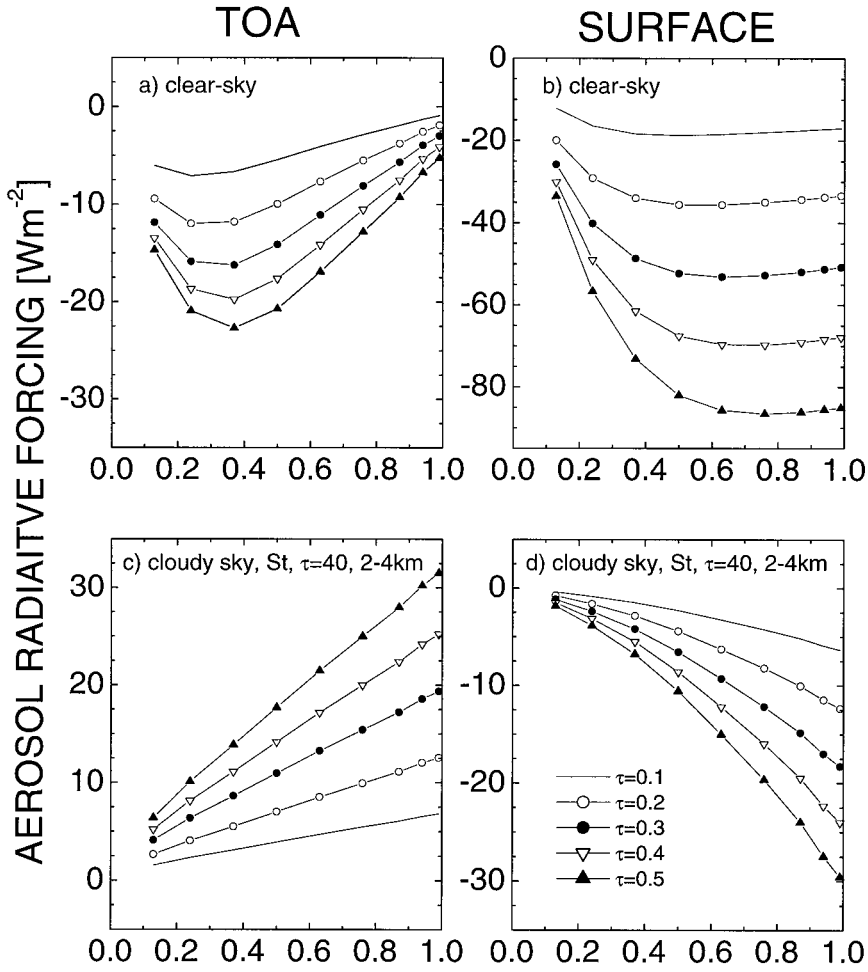

FIG. 3. Model-simulated aerosol radiative forcing under clear (a) and (b) and cloudy (c) and (d) skies at the top of the atmosphere (a) and (c) and at the surface (b) and (d). The midlatitude summer model atmosphere with a continental type of model aerosol and a St model cloud are assumed. The amount of aerosol loading is indicated on the plots.

cloudy and cloudless atmospheres in hazy conditions. The CRF ratio also decreases with increasing aerosol optical depth. Under normal circumstances, the effect may not be very significant. For example, the difference in CRF for aerosol optical depth of 0 and 0.2 is of the order of 10∼15 W m^{-2} at the TOA and 20–25 W m^{-2} at the surface. However, for heavy aerosol loading, aerosol effect may not be negligible, especially for the CRF ratio. The largest difference in CRF ratio exceeds 0.2 out of a mean value of ∼0.8 shown in Fig. 4c. Therefore, even if aerosol amount remains a constant for clear and cloudy conditions, the resulting CRF ratio is not an inherent property of cloud absorption and thus comparisons of R over different aerosol environments for interpreting the effect of cloud on solar absorption need to be cautious. The second scenario deals with different amounts of aerosol loadings under clear and cloudy conditions. For simplicity, Fig. 5 shows the variation of the difference in CRF ratio (ΔR) as defined in Eq. (5) with aerosol optical depth (τ) that is different for clear-sky and cloudy conditions. The differences represent averaged values over all ranges of SZA. The rate of correction in R is about 0.05 per $\Delta\tau = 0.1$. When τ for cloudy-sky is larger than for clear-sky, the observed CRF ratio is overestimated, and vice versa.

b. Water vapor effect

Like aerosol, variations in water vapor could impede the determination of CRF. Similar to CRF, we may refer to the SW radiative effect of water vapor as water vapor radiative forcing (WRF). If WRF is not accounted for properly, CRF derived from observations may include a component of WRF. To better understand such an effect, WRF was simulated under clear and cloudy conditions at both the surface and TOA levels. Following the definition of CRF, WRF is defined as the difference in net flux for a system (TOA or surface) with and without water vapor. Figure 6 presents the results of simulations for a varying amount of water vapor. It

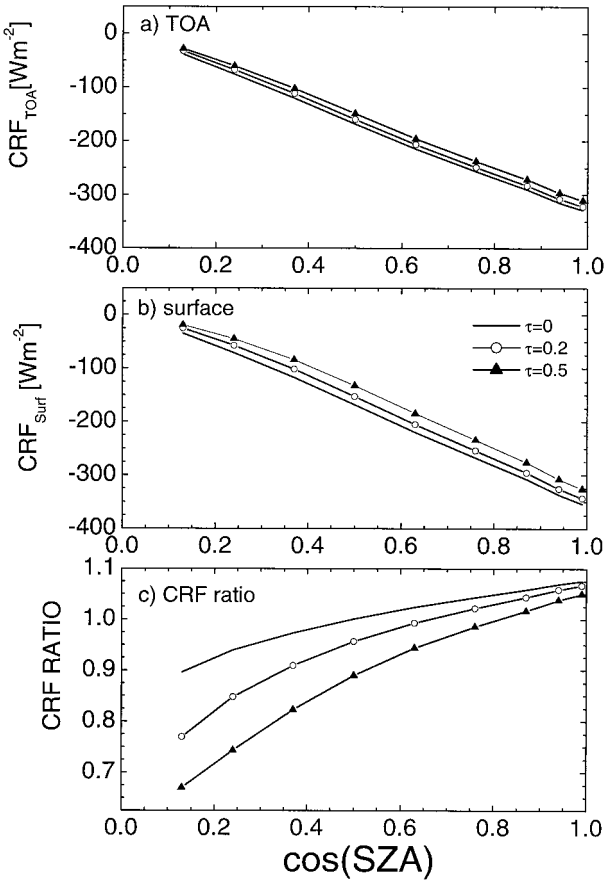

FIG. 4. Model-computed cloud radiative forcing at the TOA (a), at the surface (b), and their ratio (surface/TOA) (c) for different amounts of aerosol optical depth. Discrepancies among the curves indicate the effect of aerosol (same for clear and cloudy skies) on the determination of CRF and its ratio.

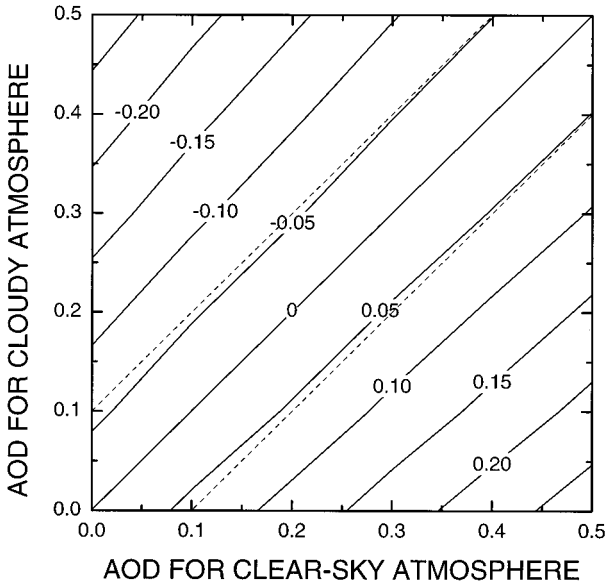

FIG. 5. The correction to the cloud radiative forcing ratio due to different amounts of aerosol contained in clear and cloudy atmospheres. Two dashed lines define the area where differences in aerosol optical thickness between cloudy and clear-sky scenes $\Delta\tau < 0.1$. Values were averaged over all ranges of SZA.

shows that under the clear-sky condition WRF is negative at the surface and positive at the TOA, implying a SW cooling and SW warming effect, respectively, at the surface and for the surface–atmosphere system. Yet, the magnitude of surface cooling is about twice that of TOA warming, also noted by Chou et al. (2000, manuscript submitted to *J. Geophys. Res.*). Note that the magnitude of clear-sky WRF depends not only on water vapor amount but also on surface albedo. As surface albedo increases, the magnitude of TOA WRF is amplified and that of surface WRF is reduced. TOA WRF for cloudy conditions is significantly larger and more sensitive to water vapor amount than that for clear conditions due to enhanced absorption of the backscattered solar radiation by water vapor above the cloud top, which may not be the case for high thick clouds though. For surface WRF, it is just the opposite due to the shielding effect of the cloud layer and overlap in absorption bands by water vapor and cloud droplets. The unequal response to water vapor between clear and cloudy conditions for both TOA and surface implies that the CRF determined even for the same water vapor content under clear and cloudy conditions contains an effect of water vapor, but its magnitude is much smaller than that of cloud. Figure 7 shows the variation of CRF and its ratio with water vapor and SZA. It shows that the effect is not very large, except for dry atmospheric conditions. However, if different water vapor amounts are assumed for clear and cloudy conditions, the impact is more significant, as is shown in Fig. 8. Due to saturation of absorption of SW radiation by water vapor, the effect of unequal water vapor amounts under clear-sky and cloudy conditions is more important for a drier atmosphere. The correction in observed CRF ratio ΔR may be over 0.35 for a difference of 1 cm in water vapor content (PW = 1 cm for cloudy and 0.0 cm for clear conditions). Unlike aerosol, whose content under clear and cloudy conditions may remains the same, water vapor content for clear and cloudy skies is generally different, the former being less than the latter as can be seen from Table 2. Therefore, only half of the Fig. 8 above the diagonal is physically meaningful, suggesting negative corrections for observed CRF ratios.

5. Determination of CRF from satellite and surface observations

The above analyses clearly show that the accuracy of CRF may be affected significantly by the clear-sky reference values. A proper determination of CRF entails delicate identification of clear skies and corrections to account for clear-sky variations as well as discrepancies between clear and cloudy conditions. The scene identification process should eliminate all cloud-contami-

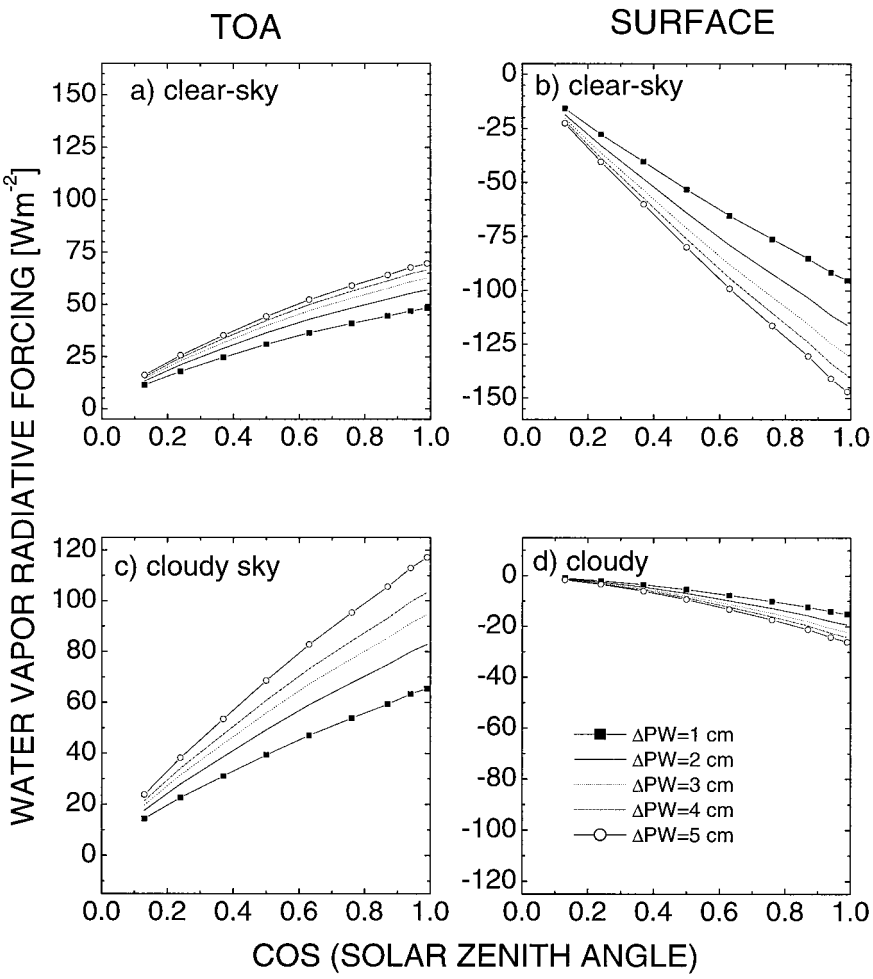

FIG. 6. Similar to Fig. 3 but for water vapor. The basic state of the atmosphere contains no water vapor.

nated scenes, and at the same time should not select only overly dry and/or clean scenes. This is a rather challenging task in practice without much ancillary information.

The following analyses of observational data demonstrate the sensitivities of CRF at the surface and TOA as well as their ratio to the selection of clear scenes. A series of screening tests were applied to matched satellite and surface data, using the method proposed by Chou and Zhao (1997):

1) The satellite scene is identified as being ''clear over land'' to assure a generally clear sky over a large area;
2) the standard deviations of direct flux $\sigma_{\mathrm{Dir}} < 20$ W m^{-2} and that of diffuse flux $\sigma_{\mathrm{Dif}} < 7$ W m^{-2} during a 30-min interval to eliminate more variable cloudy scenes; and
3) the ratio diffuse/total is less than 0.6 to remove thick clouds but retain tenuous aerosol.

The above preliminary tests remove bulk clouds, but small residual clouds may still exist. A further test is applied to direct fluxes. For the selected data, direct fluxes are fitted with a 3d-order polynomial $F^{\mathrm{DIR}}_{\mathrm{appr}}$ with respect to μ and the standard deviation σ_{DIR} of the residual (differences between observed and fitted direct flux values) is computed. Data satisfying the following condition are considered as being contaminated by clouds:

$$(F^{\mathrm{DIR}}_{\mathrm{appr}} - F^{\mathrm{DIR}}) > (\sigma_{\mathrm{DIR}} + \sigma_{\mathrm{DIR}}\mu). \qquad (7)$$

Note that the last test may be implemented iteratively. The clear data points selected after applying criteria 1–3 and the 1-step iteration according to Eq. (7) are shown in Fig. 9, in comparison with the original data without screening. The measurements were made at a Canadian AES station in Winnipeg, Manitoba, Canada. The figure shows that the bulk, if not all, of cloudy and cloud-contaminated data are removed. The remaining variability is caused mainly by changes in clear-sky condition. The curves in Fig. 9 are the modeling results for total surface downward and TOA net fluxes over a grass-

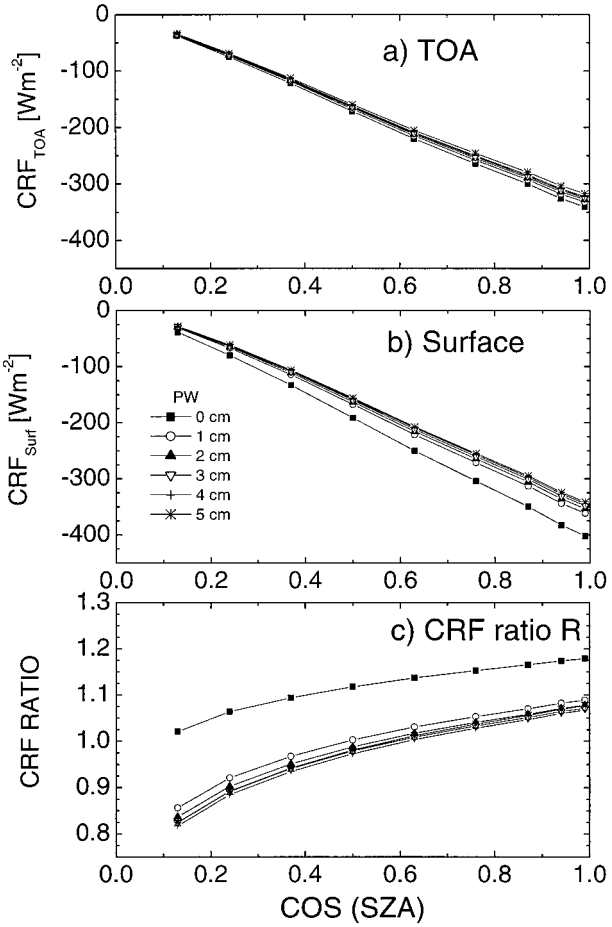

FIG. 7. Similar to Fig. 4 but for water vapor.

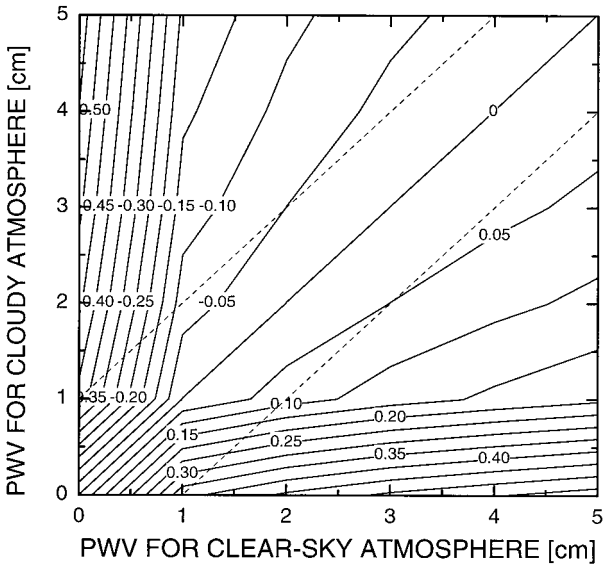

FIG. 8. Similar to Fig. 5 but for water vapor. Dashed lines confine the area where $\Delta PW < 1$ cm.

land surface for a range of plausible atmospheric conditions. The close overlap between the model curves and observation points bolsters certain confidence in the selection procedure. Consistent with the modeling results, TOA fluxes are much less variable than those at the surface. If the fluctuations were induced by clouds, the variability would be comparable for the surface and at the TOA CRF.

As was demonstrated earlier, it is important to include hazy and humid atmospheric states in the determination of clear-sky reference values for deriving CRF. Otherwise, clear-sky offset would be biased toward higher values leading to overestimation of CRF at the surface level, although it has negligible impact on TOA CRF. Figure 10 illustrates this clearly and shows the variations of CRF at the surface and TOA and their ratio with the number of iterations. As the number of iterations increases, the atmosphere selected becomes drier and cleaner, resulting in enhanced surface CRF, but TOA CRF remains essentially intact so that their ratio shows a significant increasing trend with the number of iteration. After 5 iterations, the overestimation amounts to nearly 20%.

Bearing these in mind, CRF at the surface and TOA and their ratio are derived from the matched satellite and ground data collected at 10 stations located in Canada, the United States, and other part of the world. The CRF ratios range typically from 0.88 to 1.13, as shown in Table 3. Therefore, clouds exert a moderate influence on the absorption of solar radiation in the atmospheric column, in accordance with our previous findings using different datasets (Li et al. 1995, 1999). The estimates from three different satellites are rather compatible. Note that these estimates do not account for discrepancies in the atmospheric state between clear and cloudy skies. While it is difficult to fully account for the differences because of a lack of knowledge on aerosol loading under clear and cloudy conditions, it is possible to grossly correct for the effect of water vapor differences between clear and cloudy skies. Correction for such differences was made by substituting actual amounts of PW observed under all-sky conditions into an empirical relation between PW and solar irradiance established under clear-sky conditions for a given solar zenith angle. To this end, lookup tables (LUTs) were developed from all clear-sky measurements of duration longer than 180 min for each day. Each LUT corresponds to an interval of 0.25 cm for PW and 0.05 for cos (SZA). Intermediate values were derived by interpolation. The principles of the correction are the same as those employed by Arking (1999b), who applied linear multiple regression to alleviate the difference due to water vapor loading. The advantage of the LUT approach resides in that it is not limited to any particular format of the dependence function. Figure 11 shows a comparison of surface to TOA CRF ratio derived from the two methods. Since cloudy atmosphere usually has higher contents of water vapor, surface ''clear-sky'' ref-

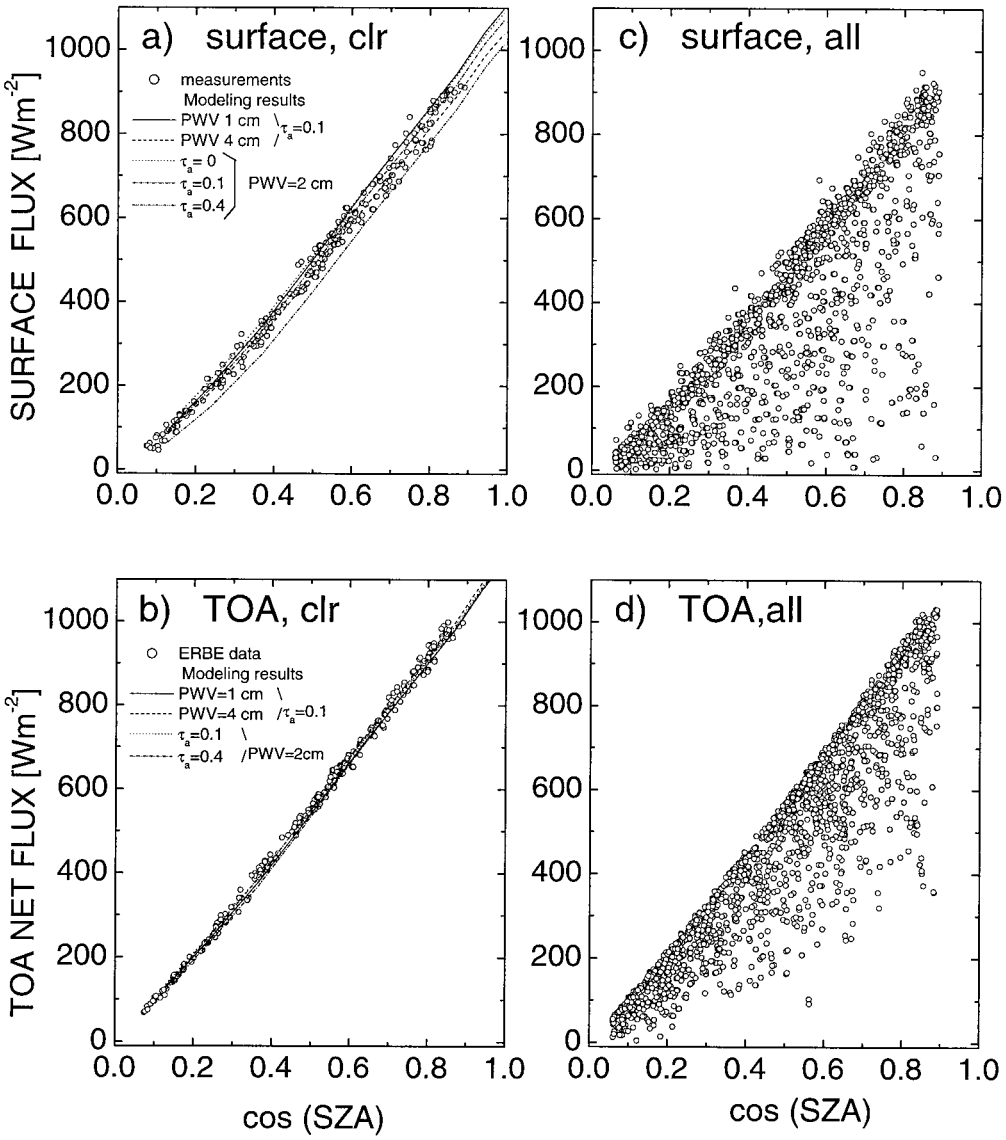

FIG. 9. Surface total downward (a) and TOA net solar fluxes (b) for clear-sky scenes after cloud screening, in comparison to the original data (c) and (d) for Winnipeg, 1988–90. The curves are model-computed fluxes for different amounts of precipitable water and aerosol loading.

erence fluxes derived from LUT are smaller, leading to smaller magnitudes of surface CRF and the CRF ratio. The exception is Port Hardy (Vancouver Island, British Columbia, Canada) and ScaRaB data, where the number of clear-sky points after screening was very small (16 points) and thus contained larger uncertainties.

6. Summary

Cloud radiative forcing (CRF) is a simple but effective parameter that has been widely employed in studying cloud–radiation interaction and diagnosing general circulation models. Although even a cursory use of CRF is capable of describing the bulk effects of clouds on the earth's radiation budget, a more quantitative evaluation and further insight into the complex relationship between cloud and radiation require more accurate determination of CRF. When CRF at the surface and at the top of the atmosphere (TOA) are combined to study the net effect of clouds on the atmospheric shortwave radiation budget, it becomes more vulnerable to the uncertainties in the CRF. CRF represents, in principle, the sole effect of clouds on the radiation budget, but in practice, observational determination of CRF suffers from uncertainties due to factors other than clouds. The variability in the atmospheric background condition is a major source of errors that are addressed in this investigation.

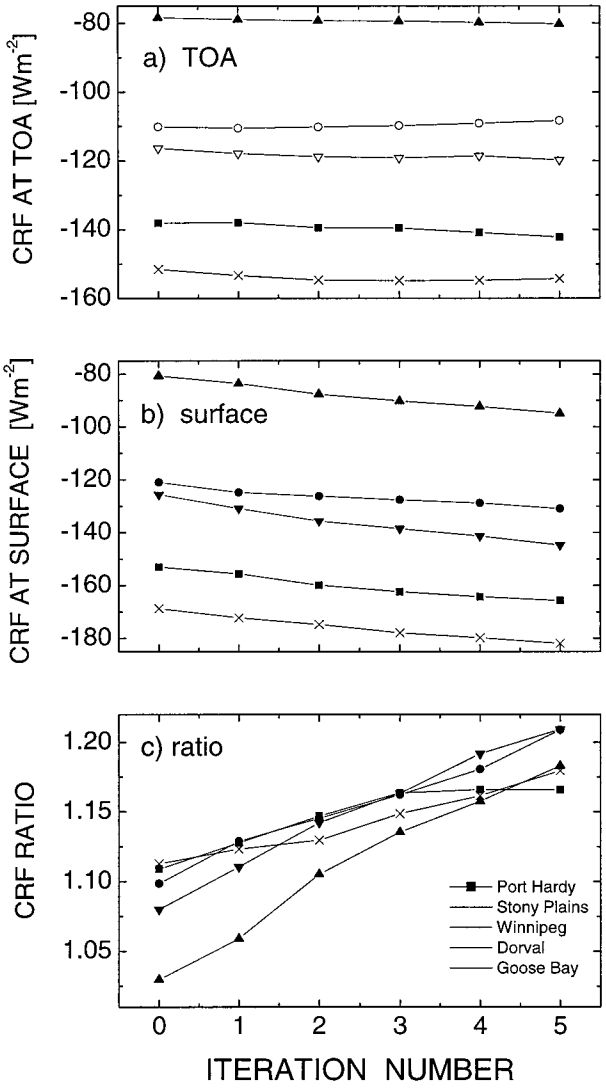

FIG. 10. Cloud radiative forcing at the TOA (a), surface (b), and their ratio (c) determined by following the different number of iterations in the clear-sky selection procedure.

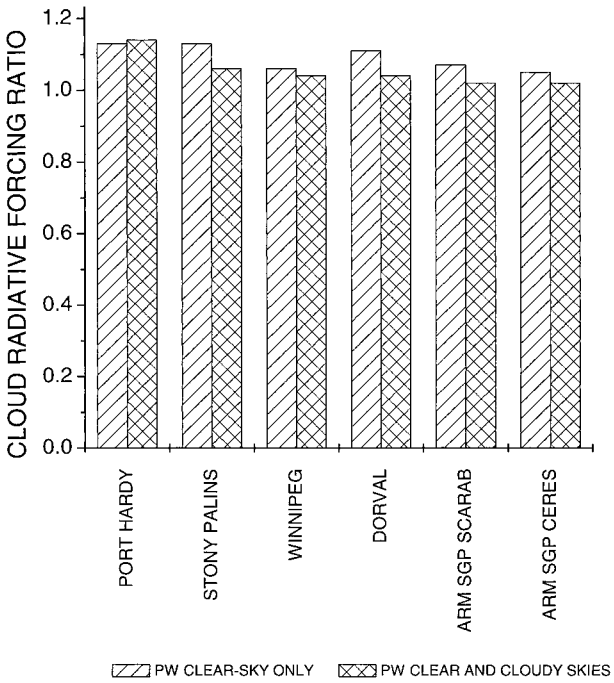

FIG. 11. A comparison of the ratios of cloud radiative forcing derived using clear-sky data only and both clear and cloudy skies for determining the background radiative fluxes.

Shortwave CRF is defined as the difference in the net SW flux of a system between actual sky conditions and clear-sky conditions. Note that clear-sky radiative flux here is not constant. Fluctuations in clear-sky flux are caused by the radiative effects of such atmospheric constituents as water vapor and aerosol that should not be confused with the effects of clouds. By means of model simulation, atmospheric radiative effects caused by water vapor and aerosol are computed and discussed, in the context of their impact on the determination of CRF. For conservative scattering aerosol, its radiative forcing at the TOA and at the surface are identical and have little or no effect on CRF. For absorbing aerosols, their radiative effect at the surface may be considerably larger than at the TOA, yielding different influences on CRF

TABLE 3. Surface and TOA cloud radiative forcing and their ratio derived from ERBE, ScaRaB, and CERES satellites and ground observations.

Station name	ERBE			ScaRaB			CERES		
	R	CRFs	CRF_{TOA}	R	CRFs	CRF_{TOA}	R	CRFs	CRF_{TOA}
1. Port Hardy (AES)	1.13	−155.6	−138.0	1.03	−166.8	−162.3	—	—	—
2. Stony Plain (AES)	1.13	−124.8	−110.5	1.10	−121.7	−110.9	—	—	—
3. Winnipeg (AES)	1.06	−83.6	−78.9	1.00	−122.5	−122.5	—	—	—
4. Dorval (AES)	1.11	−130.9	−117.9	1.02	−152.1	−149.9	—	—	—
5. Goose Bay (AES)	1.12	−172.2	−153.3	0.97	−172.7	−177.4	—	—	—
6. DOE ARM SGP CF (Oklahoma)	—	—	—	1.07	−95.30	−89.3	1.05	−93.4	−89.7
7. Boulder (SURFRAD)	—	—	—	0.89	−107.7	−120.9	1.02	−109.3	−106.3
8. Bondville (SURFRAD)	—	—	—	—	—	—	0.88	−151.7	−163.1
9. Goodwin Creek (SURFRAD)	—	—	—	—	—	—	1.10	−128.2	−116.8
10. Payerne (BSRN)	—	—	—	0.91	−123.2	−135.7			

at the two levels. This poses a challenge in the interpretation of CRF ratio in terms of cloud absorption. Depending on the strength of aerosol absorption, aerosol forcing at the TOA may be positive or negative under clear-sky conditions, while in cloudy conditions it is generally positive. At the surface, aerosol forcing is always negative and of much larger magnitude under clear conditions than under cloudy scenes. The unequal effects of aerosol forcing under clear and cloudy conditions introduce uncertainties in the CRF, whereas the unequal influences of aerosol on surface and TOA CRF incur uncertainties in using CRF ratio to study cloud absorption. The radiative effect of water vapor and its influence is similar, in nature, to that of aerosol with some exceptions. One exception is that the water vapor effect at the TOA is significantly larger under cloudy conditions than under clear ones due to additional absorption for radiation scattered back to space. This effect is dictated by cloud-top height in combination with the profile of water vapor. Another exception is that water vapor content is usually higher for cloudy skies than for clear skies. To account for the effects of atmospheric forcing due to both aerosol and water vapor on CRF, correction factors were computed that amounted to 0.2–0.3 for dry atmospheric conditions.

The aforementioned modeling results are further reinforced by analysis of satellite observations made by the ERBE, ScaRaB, and CERES, together with ground measurements made in Canada, the United States, and Europe. It was found that surface CRF is much more sensitive to clear-sky scene identification than the TOA CRF. As more rigid cloud screening is applied, the magnitude of surface CRF keeps decreasing, whereas TOA CRF remains invariant or affected only slightly. Inaccurate cloud screening tends to artificially enhance surface CRF as it attributes the effects of atmospheric variability into the effects of clouds. Since the TOA CRF is more resistant to atmospheric variability, surface-to-TOA/CRF ratio is usually subject to overestimation. Coincidentally, any residue clouds that are not removed from the selected clear scenes also have similar effects on surface and TOA CRF. Their ratio is thus also prone to overestimation. Considering these factors, we carefully estimated CRF values at the surface and TOA as well as their ratios using data from all three satellites and corresponding ground measurements. The results indicate that observations are consistent with model prediction concerning the effect of cloud on atmospheric absorption. Cloud radiative forcing ratios are confined mostly between 0.9 and 1.1.

Acknowledgments. The study was supported by the U.S. Department of Energy under Atmospheric Radiation Measurement (ARM) Grant DE-FG02-97ER2361. The authors are grateful to Dr. H. Barker for the provision of some ground-based surface radiation data. The use of data from the ARM program, the NASA Langley Research Center EOSDIS Distributed Active Archive Center, CNES (France), NCAR–NCEP, as well as WMO BRSN and NOAA SURFRAD radiation archives should also be acknowledged. We are thankful to Dr. J. Michalsky (Atmospheric Sciences Research Center, The University at Albany, State University of New York) for making available a dataset used for retrieving aerosol optical depth over the ARM SGP site in Oklahoma.

REFERENCES

Arking, A., 1991: The radiative effects of clouds and their impact on climate. *Bull. Amer. Meteor. Soc.,* **72,** 795–813.

——, 1999a: Bringing climate models into agreement with observations of atmospheric absorption. *J. Climate,* **12,** 1589–1600.

——, 1999b: The influence of clouds and water vapor on atmospheric absorption. *Geophys. Res. Lett.,* **26,** 2729–2732.

Augustine, J. A., J. J. DeLuisi, and C. N. Long, 2000: SURFRAD—A national surface radiation budget network for atmospheric research. *Bull. Amer. Meteor. Soc.,* **81**, 2341–2357.

Barker, H. W., Z. Li, and J.-P. Blanchet, 1994: Radiative characteristics of the Canadian Climate Centre second-generation general circulation model. *J. Climate,* **7,** 1070–1091.

——, T. J. Curtis, E. Leontieva, and K. Stamnes, 1998: Optical depth of overcast cloud across Canada: Estimates based on surface pyranometer and satellite measurements. *J. Climate,* **11,** 2980–2994.

Barkstrom, B., E. Harrison, G. Smith, R. Green, J. Kibler, R. Cess, and the ERBE Science Team, 1989: Earth Radiation Budget Experiment (ERBE) archival and April 1985 results. *Bull. Amer. Meteor. Soc.,* **70,** 1254–1262.

Bush, B. C., F. P. J. Valero, A. S. Simpson, and L. Bignone, 2000: Characterization of thermal effects in pyranometers: A data correction algorithm for improved measurement of surface insolation. *J. Atmos. Oceanic Technol.,* **17,** 165–175.

Cess, R. D., and Coauthors, 1995: Absorption of solar radiation by clouds: Observations versus models. *Science,* **267,** 496–499.

——, and Coauthors, 1997: Comparison of the seasonal change in cloud-radiative forcing from atmospheric general circulation models and satellite observations. *J. Geophys. Res.,* **102,** 16 593–16 603.

——, M. Zhang, F. P. J. Valero, S. K. Pope, A. Bucholtz, B. Bush, C. S. Zender, and J. Vitko Jr., 1999: Absorption of solar radiation be the cloudy atmosphere: Further interpretations of collocated aircraft measurements. *J. Geophys. Res.,* **104,** 2059–2066.

Charlock, T. P., and V. Ramanathan, 1985: The albedo field and cloud radiative forcing produced by a general circulation model with internally generated cloud optics. *J. Atmos. Sci.,* **42,** 1408–1429.

Chou, M.-D., and W. Zhao, 1997: Estimation and model validation of surface solar radiation and cloud radiative forcing using TOGA COARE measurements. *J. Climate,* **10,** 610–620.

——, ——, and S.-H. Chou, 1998: Radiation budgets and cloud radiative forcing in the Pacific warm pool during TOGA COARE. *J. Geophys. Res.,* **103,** 16 967–16 977.

——, P.-K. Chan, and M.-H. Yan, 2000: A sea surface radiation data set for climate applications in the tropical western Pacific and South China Sea. *J. Geophys. Res.,* in press.

Dutton, E. G., T. L. Stoffel, and J. J. Michalsky, 1999: Thermal offset errors in solar diffuse measurements with some commercial pyrometers. *Proc. Ninth Atmospheric Radiation Measurement (ARM) Science Team Meeting,* San Antonio, TX, ARM Program, 2 pp. [Available online at http://www.arm.gov/docs/documents/technical/conf_9903/.]

Haeffelin, M., A. M. Smith, and J. R. Mahan, C. K. Rutledge, and S. Kato, 1999: Surface shortwave radiation measurements: Experimental tests and numerical simulations of pyranometers. *Proc. Ninth Atmospheric Radiation Measurement (ARM) Science Team Meeting,* San Antonio, TX, ARM Program. [Available

online at http://www.arm.gov/docs/documents/technical/conf_9903/.]

Harrison, E. F., P. Minnis, B. R. Barkstrom, V. Ramanathan, R. D. Cess, and G. G. Gibson, 1990: Seasonal variation of cloud radiative forcing derived from the Earth Radiation Budget Experiment. *J. Geophys. Res.,* **95,** 18 687–18 703.

Harrison, L., J. Michalsky, and J. Berndt, 1994: Automated multifilter rotating shadow-band radiometer: An instrument for optical depth and radiation measurements. *Appl. Opt.,* **33,** 5118–5125.

Hartman, D. L., V. Ramanathan, A. Berroir, and G. E. Hunt, 1986: Earth radiation budget data and climate research. *Rev. Geophys.,* **24,** 439–468.

Imre, D. G., E. H. Abramson, and P. H. Daum, 1996: Quantifying cloud-induced shortwave absorption: An examination of uncertainties and recent arguments for large excess absorption. *J. Appl. Meteor.,* **35,** 1991–2010.

Ji, Q., and S.-C. Tsay, 2000: On the dome effect of Eppley pyrgeometers and pyranometers. *Geophys. Res. Lett.,* **27,** 971–974.

Kalnay, E., and Coauthors, 1996: The NCEP/NCAR 40-Year Reanalysis Project. *Bull. Amer. Meteor. Soc.,* **77,** 437–471.

Kandel, R., and Coauthors, 1998: The ScaRaB earth radiation budget dataset. *Bull. Amer. Meteor. Soc.,* **79,** 765–783.

Kneizys, F. X., E. P. Shettle, L. W. Abreau, J. Chetwynd, G. Anderson, W. Gallery, J. Selby, and S. Clough, 1988: User's guide to LOWTRAN-7. Air Force Geophysics Laboratory Tech. Rep. AFGL-TR-88-0177, 140 pp. [Available from AFGL (OPI), Hanscom AFB, MA 01731.]

Li, Z., 1998: Influence of absorbing aerosols on the inference of solar surface radiation budget and cloud absorption. *J. Climate,* **11,** 5–17.

——, and H. G. Leighton, 1993: Global climatologies of solar radiation budgets at the surface and in the atmosphere from 5 years of ERBE data. *J. Geophys. Res.,* **98,** 4919–4930.

——, and L. Garand, 1994: Estimation of surface albedo from space: A parameterization for global application. *J. Geophys. Res.,* **99,** 8335–8350.

——, H. W. Barker, and L. Moreau, 1995: The variable effect of clouds on atmospheric absorption of solar radiation. *Nature,* **376,** 486–490.

——, L. Moreau, and A. Arking, 1997: On solar energy disposition: A perspective from observation and modeling. *Bull. Amer. Meteor. Soc.,* **78,** 53–70.

——, A. Trishchenko, H. W. Barker, G. L. Stephens, and P. T. Partain, 1999: Analysis of Atmospheric Radiation Measurement (ARM) program's Enhanced Shortwave Experiment (ARESE) multiple data sets for studying cloud absorption. *J. Geophys. Res.,* **104,** 19 127–19 134.

Liou, K. N., 1992: *Radiation and Cloud Processes in the Atmosphere: Theory, Observation, and Modeling.* Oxford University Press, 487 pp.

Long, C. N., and T. P. Ackerman, 1996: Detection of clear skies using total and diffuse shortwave irradiance: Calculations of shorwave cloud radiaitve forcing and clear-sky diffuse ratio. *Proc. Sixth Atmospheric Radiation Measurement (ARM) Science Team Meeting,* San Antonio, TX, ARM Program, 179–183.

Masuda, K., H. G. Leighton, and Z. Li, 1995: A new parameterization for the determination of solar flux absorbed at the surface from satellite measurements. *J. Climate,* **8,** 1615–1629.

Michalsky, J., E. Dutton, M. Rubes, D. Nelson, T. Stoffel, M. Wesley, M. Splitt, and J. DeLuisi, 1999: Optimal measurement of surface shortwave irradiance using current instrumentation. *J. Atmos. Oceanic Technol.,* **16,** 55–69.

Ohmura, A., and Coauthors, 1998: Baseline Surface Radiation Network (BSRN/WCRF): New precision radiometry for climate research. *Bull. Amer. Meteor. Soc.,* **79,** 2115–2136.

Ramanathan, V., R. D. Cess, E. F. Harrison, P. Minnis, B. R. Barkstrom, E. Ahmad, and D. Hartman, 1989: Cloud-radiative forcing and climate: Results from the Earth Radiation Budget Experiment. *Science,* **243,** 57–63.

——, B. Subasilar, G. J. Zhang, W. Conant, R. D. Cess, J. T. Kiehl, H. Grassl, and L. Shi, 1995: Warm pool heat budget and shortwave cloud forcing: A missing physics. *Science,* **267,** 499–503.

Rossow, W. B., and Y.-C. Zhang, 1995: Calculation of surface and top-of-atmosphere radiative fluxes from physical quantities based on ISCCP datasets: 2. Validation and first results. *J. Geophys. Res.,* **100,** 1167–1197.

Stephens, G. L., 1979: Optical properties of eight water cloud types. CSIRO Division of Atmospheric Physics Tech. Paper 36, 35 pp. [Available from CSIRO, Station Street, Aspendale, Victoria 3195, Australia.]

——, 1999: Radiative effects of clouds and water vapor. *Global Energy and Water Cycles,* K. A. Browning and R. J. Gurney, Eds., Cambridge University Press, 71–90.

——, and S.-C. Tsay, 1990: On cloud absorption anomaly. *Quart. J. Roy. Meteor. Soc.,* **116,** 671–704.

Trishchenko, A., and Z. Li, 1998a: Use of ScaRaB measurements for validating a GOES-based TOA radiation product. *J. Appl. Meteor.,* **37,** 591–605.

——, and ——, 1998b: A synergetic study of solar fluxes and aerosol properties under clear-sky conditions. *Proc. Eighth Atmospheric Radiation Measurement (ARM) Science Team Meeting,* Tucson, AZ, ARM Program, 761–765.

Valero, F. P. J., R. D. Cess, M. Zhang, S. K. Pope, A. Bucholtz, B. Bush, and J. Vitko Jr., 1997: Absorption of solar radiation by the cloudy atmosphere: Interpretations of collocated aircraft measurements. *J. Geophys. Res.,* **102,** 29 917–29 928.

WCP, 1986: A preliminary cloudless standard atmosphere for radiation computation. World Climate Program WCP-112, WMO/TD-No24, 53 pp.

Wielicki, B. A., B. R. Barkstrom, E. F. Harrison, R. B. Lee III, G. L. Smith, and J. E. Cooper, 1996: Clouds and the Earth's Radiant Energy System (CERES): An Earth Observing System experiment. *Bull. Amer. Meteor. Soc.,* **77,** 853–868.

Zender, C. S., B. Bush, S. K. Pope, A. Bucholtz, W. D. Collins, J. T. Kiehl, F. P. J. Valero, and J. Vitko Jr., 1997: Atmospheric absorption during the Atmospheric Radiation Measurement (ARM) Enhanced Shortwave Experiment (ARESE). *J. Geophys. Res.,* **102,** 29 90l–29 916.

Zhang, Y.-C., W. B. Rossow, and A. A. Lacis, 1995: Calculation of surface and top-of-atmosphere radiative fluxes from physical quantities based on ISCCP data sets, 1. Method and sensitivity to input data uncertainties. *J. Geophys. Res.,* **100,** 1149–1165.